

# Using image analysis in the study of multiphase gas absorption

P.C. Mena<sup>a</sup>, M.N. Pons<sup>b</sup>, J.A. Teixeira<sup>c</sup>, F.A. Rocha<sup>a,\*</sup>

<sup>a</sup>Departamento de Engenharia Química, Faculdade de Engenharia, Universidade do Porto, Rua Dr. Roberto Frias s/n, 4200-465 Porto, Portugal

<sup>b</sup>Laboratoire des Sciences du Génie Chimique, CNRS-ENSIC-INPL, 1, Rue Grandville, BP 451, F-54001 Nancy Cedex, France

<sup>c</sup>Centro de Engenharia Biológica – IBQF, Universidade do Minho, Campus de Gualtar, 4710-057 Braga, Portugal

Received 27 January 2004; received in revised form 24 November 2004; accepted 7 April 2005

Available online 13 June 2005

## Abstract

For the air–water–calcium alginate beads system, the effect of the presence of solids on the mass transfer characteristics in a bubble column was experimentally studied.

Volumetric liquid side mass transfer coefficient,  $k_L a$ , specific interfacial area,  $a$ , and hence liquid side mass transfer coefficient,  $k_L$ , were determined under different solid concentrations (0, 5, and 10 vol%), superficial gas velocities (up to 0.27 cm/s) and solid sizes (1.2 and 2.1 mm diameter). The bubble characteristics, namely the interfacial area, were obtained using an image analysis technique.

This technique proved to be a suitable and practical method to characterize mass transfer phenomena in bubble columns for the range of operating conditions used. The solids affect negatively  $k_L a$ , decreasing both  $a$  and  $k_L$ , the effect being more pronounced for the smaller particles. For these particles the variation of  $k_L a$  is due to the variation of its two components, while for larger particles  $k_L a$  variation is due, essentially, to changes in  $k_L$  as no significant differences in  $a$  were observed.

© 2005 Elsevier Ltd. All rights reserved.

**Keywords:** Absorption; Bubble column; Mass transfer; Multiphase reactors; Image analysis; Particles

## 1. Introduction

Bubble columns are commonly used in industry as gas–liquid and gas–liquid–solid contactors. Chemical or biochemical reactive operations, as well as the separation of mixtures by rectification, absorption, and wastewater purification, can serve as examples of their application (Hong and Brauer, 1989). Bubble columns are also gaining increasing importance in the field of biotechnology (Alvarez et al., 2000).

In multiphase systems, appearing in mechanically agitated reactors and bubble columns, gas–liquid mass transfer is most frequently the rate determining step for the overall process. Therefore, the knowledge of gas–liquid mass transfer rates characterized by volumetric liquid side mass transfer coefficients ( $k_L a$ ) is required for a reliable design of such reactors (Ozkan et al., 2000). Also a complete

understanding of the effect of the operating parameters on each component of  $k_L a$ —the liquid side mass transfer coefficient ( $k_L$ ) and the interfacial area ( $a$ )—is needed.

In three phase systems, the presence of solids is an important parameter that can have either a beneficial or undesirable influence on the mass transfer process. Thus, the effect of solid characteristics such as size, loading and surface properties on gas–liquid mass transfer has been a challenging task for researchers. Yagi and Yoshida (1974) verified that the effect of dead microorganisms on the liquid phase mass transfer coefficient  $k_L$  was negligible. However, the presence of such substances caused remarkable change in the bubble size distribution, and consequently decreased the gas holdup, the specific gas–liquid interfacial area  $a$ , and the volumetric mass transfer coefficient  $k_L a$ . Albal et al. (1983) added glass beads and oil shale particles to water in order to study the effect of solids concentration on  $k_L a$ . The solids concentration varied from 0 to 25–vol%. For low values (2–5 vol%) of the solids concentration,  $k_L a$  increased by about 10%–30% and then decreased with a further increase

\* Corresponding author. Tel.: +351 225081678; fax: +351 225081632  
E-mail address: frocha@fe.up.pt (F.A. Rocha).

in the solids concentration. Sada et al. (1986) concluded that the influence of fine suspended particles on bubble column performance depends upon the particle size. More recently, Freitas and Teixeira (2001) showed that the volumetric mass transfer coefficient diminishes with the increase in solids loading, especially for high airflow rates, due to an increase in bubble coalescence. Reductions of 40% and 70% were obtained with the introduction of 20% and 30% of solids, respectively. Solid density also affects  $k_L a$ .

Several methods exist for measuring the interfacial area in gas–liquid systems, such as photographic, light attenuation, ultrasonic attenuation, double-optical probes and chemical absorption methods. But these methods are effective only under specific conditions (Kiambi et al., 2001).

In this work, photographic and a subsequent image analysis technique was used to determine bubble characteristics such as superficial area, size and shape. Volumetric mass transfer coefficients were obtained for different gas flow rates, solids loading and size. The effect of these variables on the liquid side mass transfer coefficient ( $k_L$ ) and interfacial area ( $a$ ) was analyzed.

## 2. Experimental

### 2.1. Experimental Set-Up

In this work a bubble column was used as contact device. This is a perspex cylindrical column of 84 mm internal diameter, 3 mm thick and 600 mm high. A perspex rectangular box covers the column. The space between the two columns is filled with the liquid under study to avoid optical effects. The gas first enters a gas chamber and then passes through a sparger where bubbles are formed. The sparger consists of 13 uniformly spaced needles with an inner diameter of 0.3 mm. The shape and size of the needles ensure the formation of small and well-defined bubbles. A complete scheme of the experimental set-up is shown in Fig. 1.

To produce calcium alginate beads, first a 2% (w/v) sodium alginate solution was prepared dissolving sodium alginate in water at a temperature higher than 70°C, under strong agitation. This mixture is then dropped into a 2% (w/v) calcium chloride solution using a peristaltic pump, the calcium alginate beads being formed by ion exchange  $\text{Ca}^{2+} \leftrightarrow \text{Na}^+$  (Freitas, 2002). A slightly different and more complex set-up was used on the preparation of the smaller beads (Jourdain, 2002). A 0.45 mm outer diameter needle was used to drop the sodium alginate solution and an electric impulse generator working at 9 kV was connected to the chamber to promote very small drops that result in smaller beads.

### 2.2. Mass transfer experiments

Oxygen mass transfer runs were performed in two- and three-phase systems. Air and water were used as the gas

and liquid phases, respectively, and calcium alginate beads (with a mean diameter,  $d_p$ , of 1.2 and 2.1 mm, and a density of 1023 kg/m<sup>3</sup>) were the solid phase. The experiments were performed for several superficial gas velocities (up to 0.27 cm/s), and different solid concentrations (0, 5, 10 vol %) were tested.

Initially the liquid is deoxygenated by bubbling nitrogen. When the dissolved oxygen concentration is zero, dry air is fed into the column. At this moment the oxygen transfer process from air bubbles to the liquid begins and continues until O<sub>2</sub> concentration in the liquid phase reaches saturation. Dissolved oxygen concentration values are directly recorded on a PC, through a data acquisition board, and the dissolved oxygen concentration variation with time,  $t$ , is obtained. The mass balance for oxygen in the liquid medium is written as:

$$\frac{dC}{dt} = k_L a (C^* - C), \quad (1)$$

where  $k_L a$  is the volumetric mass transfer coefficient, and  $C^*$  and  $C$  are, respectively, the oxygen solubility and the oxygen concentration in the liquid.

Considering the liquid phase homogeneous and  $C_0$  the oxygen concentration at  $t = 0$ , the integration of the last equation leads to

$$\ln(C^* - C) = \ln(C^* - C_0) - k_L a t. \quad (2)$$

The volumetric mass transfer coefficient can now be determined by plotting  $\ln(C^* - C)$  against time. The  $k_L a$  results were not influenced by the dynamics of the oxygen electrode since, for all runs, it was verified that its response time was much smaller than the mass transfer time of the system.

### 2.3. Image analysis experiments

In order to obtain the characteristics of the bubbles, images were grabbed with a monochrome video digital camera (Sony XCD-X700), which was connected to a Matrox Meteor-II/1394 board. Sets of images (1024×768 Pixels) were recorded for varying gas velocities, solids loadings and sizes, for the same conditions used in mass transfer experiments. The most suitable lightning system was found to be backlight through a diffusing glass (Fig. 1). Then, the images were automatically treated, analyzed and several object descriptors obtained for each bubble using a program running under Visilog<sup>TM</sup> software (Noésis, France).

The image treatment consists in the procedure described below and illustrated in Fig. 2 (for air–water–calcium alginate 1 vol% system and a superficial gas velocity of 0.09 cm/s). It is based on the fact that alginate particles have a higher grey level than bubbles, although it is lower than for the background.

- Find the first peak in the histogram of the original grey-level image. This peak corresponds to the grey level of the bubbles.

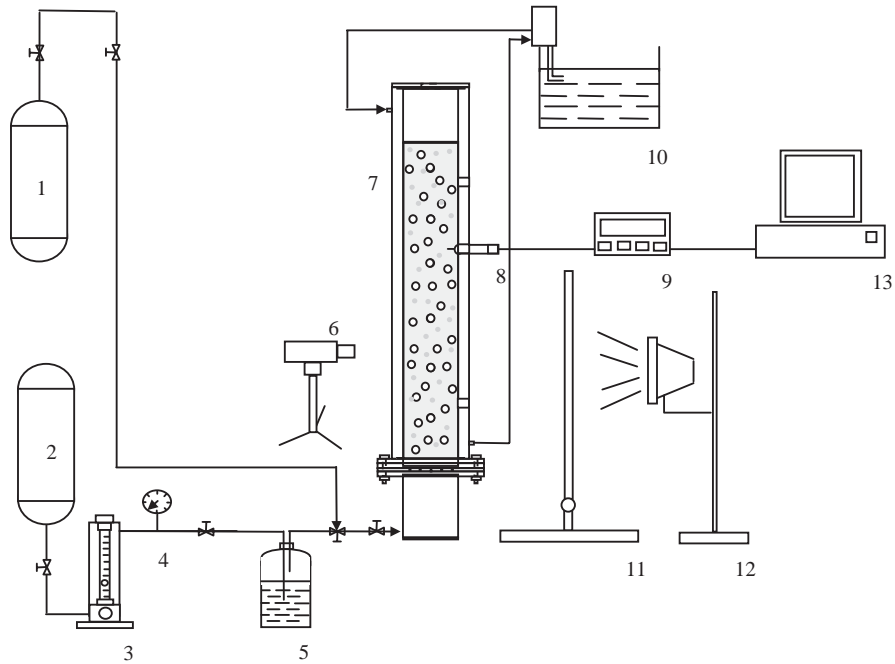


Fig. 1. Experimental set-up (1: N<sub>2</sub>, 2: Air, 3: Rotameter, 4: Manometer, 5: Humidifier, 6: Digital camera, 7: Bubble column, 8: O<sub>2</sub> probe, 9: O<sub>2</sub> conc. meter, 10: Thermostatic bath, 11: Diffuser glass, 12: Halogen lamp, 13: PC).

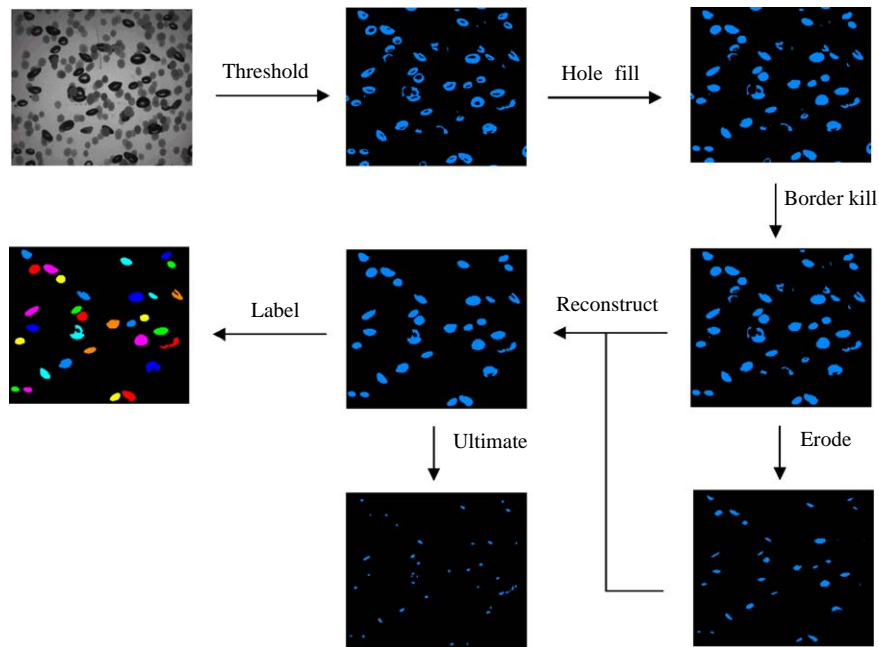


Fig. 2. Experimental set-up (1: N<sub>2</sub>, 2: Air, 3: Rotameter, 4: Manometer, 5: Humidifier, 6: Digital camera, 7: Bubble column, 8: O<sub>2</sub> probe, 9: O<sub>2</sub> conc. meter, 10: Thermostatic bath, 11: Diffuser glass, 12: Halogen lamp, 13: PC).

- Segment the grey-level image with the previous grey level as limit. Only the bubbles are selected and solids are eliminated.
- Hole fill: all the holes inside objects are filled.
- Border kill: all the objects touching the frame of the image are eliminated.
- Noise elimination applying a sequence of erosions and reconstruction. Reconstruction retrieves the original shape of the retained objects after a series of erosions that eliminates undesirable small objects.
- Labeling the image. All the objects are detected and identified.
- Ultimate searches for the ultimate eroded set. This enables to count the number of convex objects, even if some of them are touching each other, as long as the pseudo-center of each object is outside other objects.

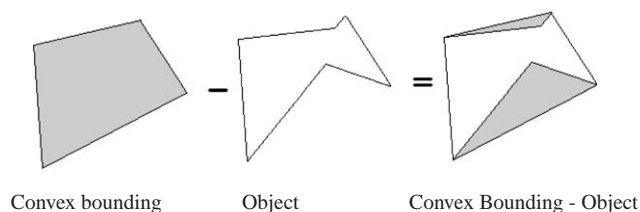


Fig. 3. Concavities of an object.

After the image treatment, several size and shape descriptors can be determined for each bubble: the projected area ( $A_p$ ) from which equivalent diameter ( $D_{eq} = 2\sqrt{A_p/\pi}$ ) can be calculated; the Feret diameters distribution, from which Feret diameter maximum ( $F_{max}$ ) and minimum ( $F_{min}$ ) are obtained (the Feret diameter is the smallest distance between two parallel tangents to the object, the tangent position being defined by the angle between them and the horizontal axis); elongation ( $F_{max}/F_{min}$ ) is also determined; the convex bounding polygon of each object is calculated and the concavity index ( $CI = A_{obj}/A_{cb}$ ) is obtained, where  $A_{obj}$  and  $A_{cb}$  are the surfaces of the object and of the convex bounding polygon, respectively (Fig. 3) (Pons et al., 1997).

It was found that  $CI > 0.99$  was a good criterion to distinguish between isolated and overlapping bubbles: overlapping induces concavities in the object and decreases the concavity index.

The change in size due to the depth of view was experimentally studied. It was found that the error in the calculation of the superficial area of the bubbles was less than 2%.

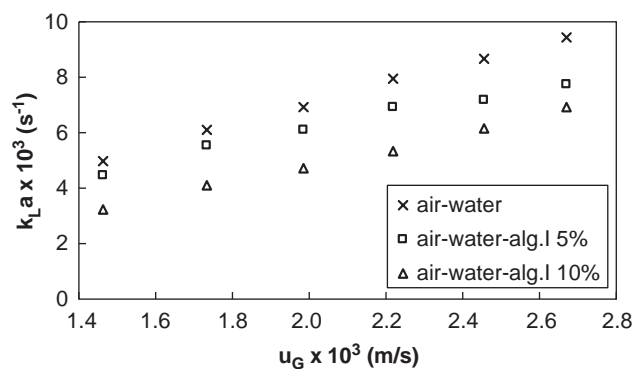
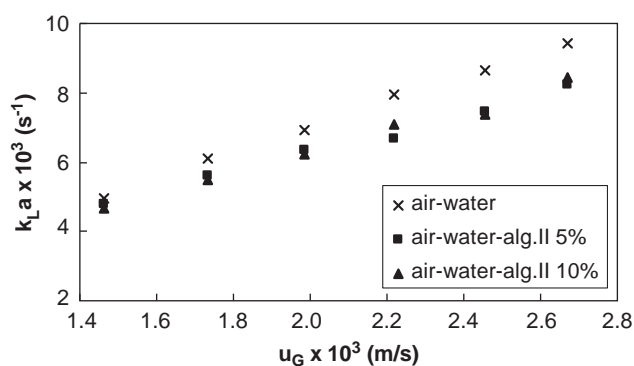
### 3. Results and discussion

#### 3.1. Mass transfer

Fig. 4 shows how  $k_{La}$  varies with superficial gas velocity,  $u_G$ , and solid loading, for calcium alginate beads of 1.2 mm diameter (alg.I). It can be seen from this figure that  $k_{La}$  increases with superficial gas velocity and decreases with the solid concentration. Further, it seems that the solid effect becomes independent from solid loading for higher gas velocities.

Zahradnik et al. (1992) studied the effect of some operating variables on hydrodynamics and mass transfer characteristics of multi-stage three-phase slurry reactors and found that the increasing concentration of solid particles (in the range 0–5 wt%) reduced the  $k_{La}$  values. Freitas and Teixeira (2001) working with a three-phase internal loop airlift reactor noticed a similar behavior for the effect of solids.

Similar experiments were performed using calcium alginate beads with a 2.1 mm size (alg.II). In this case,  $k_{La}$  also increases with superficial gas velocity (Fig. 5). The effect of the solids increases with the superficial gas velocity and is independent from solids concentration. The results shown

Fig. 4. Dependence of  $k_{La}$  on superficial gas velocity for different calcium alginate concentrations ( $d_p = 1.2$  mm).Fig. 5. Dependence of  $k_{La}$  on superficial gas velocity for different calcium alginate concentrations ( $d_p = 2.1$  mm).

in Figs. 4 and 5 seem to make evident that the smaller particles have a stronger effect on  $k_{La}$ . These results are reproducible with an average relative error of 5%. Moreover,  $k_{La}$  for 2.1 mm particles exhibits similar values (for the smaller solid loading) or higher than those obtained for 1.2 mm.

For glass spheres under 1 mm diameter in a fluidized bed, Zheng et al. (1995) found that  $k_{La}$  increases with gas velocity and decreases with solid concentration and increasing particle size.

For particles above 1 mm the effect of particle size on  $k_{La}$  changes. Kim and Kim (1990) reported that, in that range,  $k_{La}$  increases with an increase in particle size. Above 3 mm size,  $k_{La}$  is, besides, higher than in the situation without particles. The dependence of the mass transfer characteristics on particle size is also highlighted by Patwari et al. (1986) and Schumpe et al. (1989).

In order to evaluate the effect of studied parameters on  $a$  and  $k_L$  separately, the interfacial area was determined by image analysis, as already described.

#### 3.2. Bubble characteristics

The shape of the bubbles is influenced by superficial gas velocity, concentration and size of solids. In the range of used

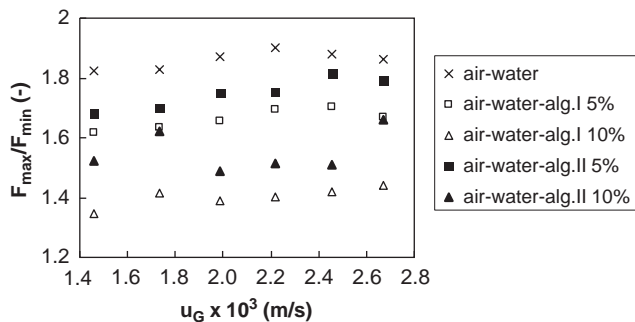


Fig. 6.  $F_{\max}/F_{\min}$  ratio for the different experimental conditions.

superficial gas velocities, the bubbles are oblate spheroids being more or less elongated according to the operating conditions. Fig. 6 shows the  $F_{\max}/F_{\min}$  ratio, which gives the bubble shape. The concentration of solids is the parameter with the strongest effect on the bubble shape. The presence of solids makes the bubbles more rounded, the effect being more pronounced for the higher solids loading and for the smaller particles, where the bubble sphericity goes near to 1.

Reese et al. (1996) studied the bubble characteristics in three-phase systems used for pulp and paper processing. They reported that the bubbles in a pulp slurry system are more flattened than in the pure liquid. In this case, however, the concentration of the particles is much smaller (from 0 to 0.25%) and the particles are fibers of varying size, shape and thickness, giving rise to a very different situation from that presented in this work.

Fig. 7 shows images of bubbles for different superficial gas velocities and solids loading, for the smaller solid size tested. These images confirm the conclusions referred above.

For all runs, several average bubble descriptors were obtained by image analysis, namely the projected area and the

Feret diameters. According to bubble characteristics, these were classified as elongated or flattened spheroids, and the respective superficial area and volume calculated according to the equations listed in Table 1 (Pereira, 1997), where  $2r_1$  corresponds to the maximum Feret diameter and  $2r_2$  to the minimum Feret diameter.

### 3.3. Interfacial area and liquid side mass transfer coefficient

The specific interfacial area,  $a$ , is calculated using the following equation:

$$a = \frac{N_b A_{sup}}{V_L} \quad (3)$$

where  $N_b$  is the number of bubbles in the column at a certain instant,  $A_{sup}$  is the mean superficial area of the bubbles and  $V_L$  is the liquid volume. The bubbles superficial area and volume are determined by the method described in the previous section. The rise velocity of bubbles is calculated from Wesselingh and Bollen (1999) and is used for determine  $N_b$ . Figs. 8 and 9 show the results for the two solid sizes used. The results are reproducible with an average relative error of 4%.

As foreseen (Kim and Kim, 1990; Vasquez et al., 2000; Quicker et al., 1984), interfacial area increases with superficial gas velocity. Even as bubbles become larger, since the number of bubbles formed increases, and in this bubble size range the rise velocity is nearly constant, the total superficial area also increases. On the other hand the solids effect is not constant. For the smaller particles one notices a significant decrease of interfacial area at the higher solids loading. This may be due to an increase of bubble coalescence leading to a decrease in total superficial area (Zahradnik et al., 1992;

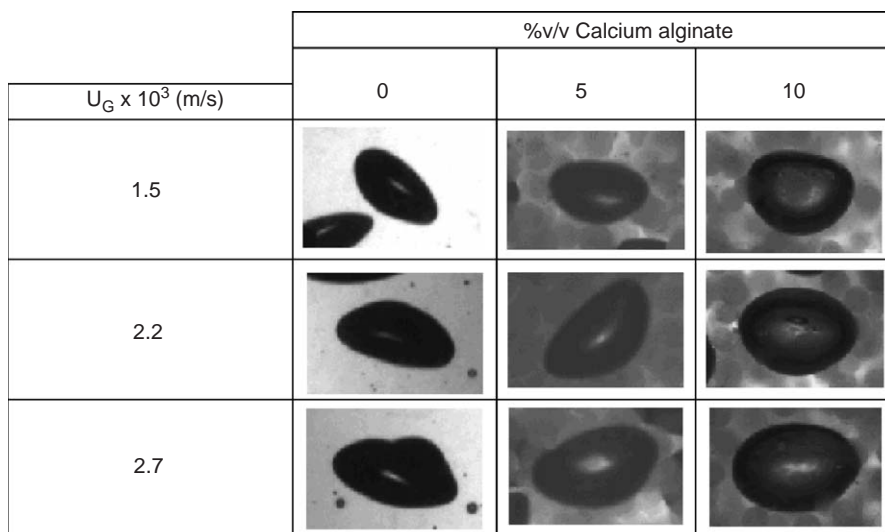


Fig. 7. Bubble examples for different superficial gas velocities and solid concentrations ( $d_p = 1.2$  mm).

Table 1  
Superficial area and volume of elongated and flattened spheroids

Spheroid	Superficial area	Volume
Elongated	$A_{\text{sup}} = 2\pi r_2^2 + 2\pi r_1^2 \sin^{-1}\left(\frac{r_2}{r_1}\right)$	$V = \frac{4}{3}\pi r_1 r_2^2$
Flattened	$A_{\text{sup}} = 2\pi r_1^2 + \pi r_1 r_2 \ln \frac{r_1+r_2}{r_1-r_2}$	$V = \frac{4}{3}\pi r_1^2 r_2$

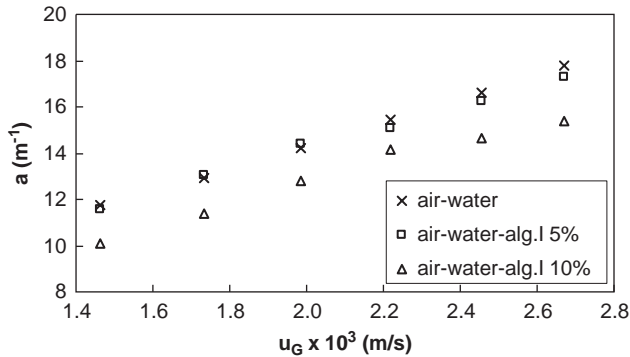


Fig. 8. Interfacial area for the smaller solid size ( $d_p = 1.2$  mm).

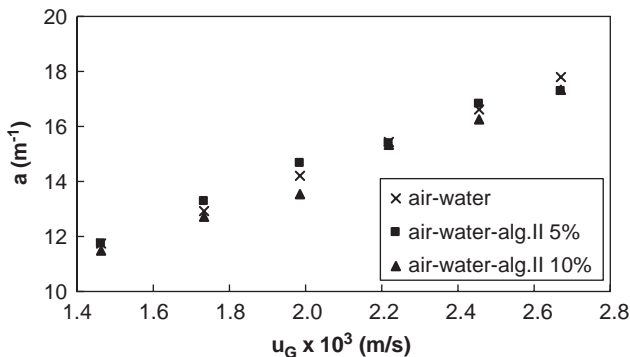


Fig. 9. Interfacial area for the larger solid size ( $d_p = 2.1$  mm).

Kim and Kim, 1990; Patwari et al., 1986). Yagi and Yoshida (1974) reported a similar effect in systems containing dead yeast cells. Both for the larger, as well as for the smaller particles at reduced concentration, the solid effect on the occurrence of the bubble coalescence phenomenon is negligible.

Liquid side mass transfer coefficient,  $k_L$ , can now be calculated from the values of  $k_L a$  and  $a$  previously determined. Figs. 10 and 11 present the results for the two solid sizes studied.  $k_L$  values reflect the previously reported values of  $k_L a$  and  $a$ . One notices a conjugate effect of the solid size and concentration on  $k_L$ . The more pronounced effect occurs for the smaller particles and at higher concentrations.

Taking into account the previous analyses, one can examine how  $a$  and  $k_L$  contribute to the  $k_L a$  behavior.

For the smaller particles, the  $k_L a$  variation is due to the simultaneous variation of  $a$  and  $k_L$  in the same direction. The presence of solids lowers the interfacial area and the mass transfer coefficient, the effect being more pronounced

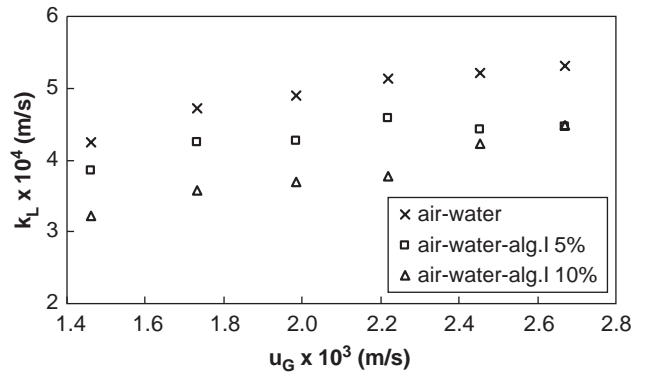


Fig. 10. Liquid side mass transfer coefficient for the smaller solid size ( $d_p = 1.2$  mm).

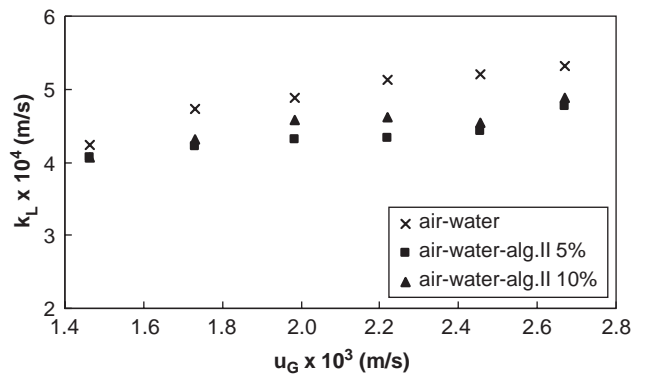


Fig. 11. Liquid side mass transfer coefficient for the larger solid size ( $d_p = 2.1$  mm).

at the higher solid concentration. For higher superficial gas velocities the solid concentration seems to have a less significant effect.

For the larger particles, the  $k_L a$  variation is almost only due to the  $k_L$  variation, which shows a negligible dependence on solids concentration. The effect of solids on interfacial area is negligible, and the effect on mass transfer coefficient seems to be more pronounced as the gas velocity increases.

#### 4. Conclusions

An image analysis technique was used to study the bubble characteristics, namely shape and size, in two phase and three phase systems. In the range of operating conditions used (superficial gas velocity and solids loading), this technique shows to be suitable and practical, as the calculated values of the specific interfacial area reproducible.

The solids present a negative effect on  $k_L a$ , volumetric liquid side mass transfer coefficient. This effect depends on the solid concentration for the smaller particles, while for the larger particles that is not evident. The effect of particle size on  $k_L a$  is significant for the higher solid concentration,

but for the smaller solid concentration particle size has no remarkable effect.

The bubble shape is also affected by the presence of the solid phase. The bubbles become more rounded as solid concentration increases and solid size decreases.

The effect of the solid phase on  $k_L a$  was separated in its components,  $a$  and  $k_L$ . The image analysis results show that, for the higher solid concentration and the smaller particle size, the solids decrease the total interfacial area, while for the other situations no significant effect occurs. This suggests the occurrence of bubble coalescence phenomena in the first case.

Calculating  $k_L$  from the experimental values of  $a$  and  $k_L a$ , one can conclude that  $k_L$  increases with superficial gas velocity and is affected negatively by the presence of solids. The effect of solid concentration is important for the smaller particles.

Finally one can infer that the  $k_L a$  variation is due to the simultaneous variations of  $a$  and  $k_L$  in the same direction for smaller particles, while for the larger particles that variation is almost only due to the  $k_L$  variation.

## Acknowledgements

This work was supported by Fundação para a Ciência e Tecnologia—contract POCTI/EQU/45194/2002, and program SFRH/BD/3427/2000.

## References

- Albal, R.S., Shah, Y.T., Schumpe, A., 1983. Mass transfer in multiphase agitated contactors. *Chemical Engineering Journal* 27, 61–80.
- Álvarez, E., Sanjurjo, B., Cancela, A., Navaza, J.M., 2000. Mass transfer and influence of physical properties of solutions in a bubble column. *Chemical Engineering Research and Design* 78 (A), 889–893.
- Freitas, C., 2002. *Biorreactores multifásicos – Caracterização hidrodinâmica e de transferência de massa*. Ph.D. Thesis, Universidade do Minho, Portugal.
- Freitas, C., Teixeira, J.A., 2001. Oxygen mass transfer in a high solids loading three-phase internal-loop airlift reactor. *Chemical Engineering Journal* 84 (1), 57–61.
- Hong, W.-H., Brauer, H., 1989. Gas-liquid mass transfer in bubble-column reactors. *International Chemical Engineering* 29 (3), 388–434.
- Jourdain, C., 2002. *Les spheroids tumoraux multicellulaires—Analyse par traitement d'image, chimiosensibilité, encapsulation de cellules tumorales humaines*. M. Sc. Thesis, Centre Alexis Vautrin, Vandoeuvre-Lès-Nancy, France.
- Kiambi, S.L., Duquenne, A., Delmas, H., 2001. Measurements of local interfacial area: application of bi-optical fibre technique. *Chemical Engineering Science* 56, 6447–6453.
- Kim, J.O., Kim, S.D., 1990. Gas-Liquid mass transfer in a three-phase fluidized bed with floating bubble breakers. *The Canadian Journal of Chemical Engineering* 68, 368–375.
- Ozkan, O., Calimli, A., Berber, R., Oguz, H., 2000. Effect of inert particles at low concentrations on gas-liquid mass transfer in mechanically agitated reactors. *Chemical Engineering Science* 55, 2737–2740.
- Patwari, A.N., Nguyen-Tien, K., Schumpe, A., Deckwer, W.-D., 1986. Three-Phase fluidized beds with viscous liquid: hydrodynamics and mass transfer. *Chemical Engineering Communications* 40, 49–65.
- Pereira, I., 1997. *Estudos de transferência de oxigênio em colunas de borbulhamento*. Ph.D. Thesis, Faculdade de Engenharia, Universidade do Porto, Portugal.
- Pons, M.N., Vivier, H., Dodds, J., 1997. Particle shape characterization using morphological descriptors. *Particle & Particle Systems Characterization* 14, 272–277.
- Quicker, G., Schumpe, A., Deckwer, W.-D., 1984. Gas-liquid interfacial areas in a bubble column with suspended solids. *Chemical Engineering Science* 39 (1), 179–183.
- Reese, J., Jiang, P., Fan, L.-S., 1996. Bubble characteristics in three-phase systems used for pulp and paper processing. *Chemical Engineering Science* 51 (10), 2501–2510.
- Sada, E., Kumazawa, H., Lee, C.H., 1986. Influences of suspended fine particles on gas holdup and mass transfer characteristics in a slurry bubble column. *A.I.Ch.E. Journal* 32 (5), 853–856.
- Schumpe, A., Deckwer, W.-D., Nigam, K.D.P., 1989. Gas-Liquid mass transfer in three-phase fluidized beds with viscous pseudoplastic liquids. *The Canadian Journal of Chemical Engineering* 67, 873–877.
- Vasquez, G., Cancela, M.A., Riverol, C., Alvarez, E., Navaza, J.M., 2000. Determination of interfacial areas in a bubble column by different chemical methods. *Industrial Engineering Chemistry Research* 39, 2541–2547.
- Wesselingh, J.A., Bollen, A.M., 1999. Single particles, bubbles and drops: Their velocities and mass transfer coefficients. *Chemical Engineering Research Design* 77 (Part A), 89–96.
- Yagi, H., Yoshida, F., 1974. Oxygen absorption in fermenters-effects of surfactants, antifoaming agents, and sterilized cells. *Journal of Fermentation Technology* 52 (12), 905–916.
- Zahradnik, J., Drápal, L., Kastánek, F., Reznickova, J., 1992. Hydrodynamic and mass transfer characteristics of sectionalized aerated slurry reactors. *Chemical Engineering and Processing* 31, 263–272.
- Zheng, C., Chen, Z., Feng, Y., Hofman, H., 1995. Mass transfer in different flow regimes of three-phase fluidized beds. *Chemical Engineering Science* 50 (10), 1571–1578.